DISCLAIMER

This report was prepared as an account of work sponsored by an agency of the United States Government. Neither the United States Government nor any agency thereof, nor any of their employees, makes any warranty, express or implied, or assumes any legal liability or responsibility for the accuracy, completeness, or usefulness of any information, apparatus, product, or process disclosed, or represents that its use would not infringe privately owned rights. Reference herein to any specific commercial product, process, or service by trade name, trademark, manufacturer, or otherwise does not necessarily constitute or imply its endorsement, recommendation, or favoring by the United States Government or any agency thereof. The views and opinions of authors expressed herein do not necessarily state or reflect those of the United States Government or any agency thereof. Reference herein to any social initiative (including but not limited to Diversity, Equity, and Inclusion (DEI); Community Benefits Plans (CBP); Justice 40; etc.) is made by the Author independent of any current requirement by the United States Government and does not constitute or imply endorsement, recommendation, or support by the United States Government or any agency thereof.

INL/RPT-22-69432

Data Mining – Image Analysis of Radiography for Zr Redistribution

September 2022

Interim Report

Andrei Gribok and Doug Porter

Idaho National Laboratory

INL is a U.S. Department of Energy National Laboratory
operated by Battelle Energy Alliance, LLC

INL/RPT-22-69432

Data Mining – Image Analysis of Radiography for Zr Redistribution

Interim Report

Andrei Gribok and Doug Porter

September 2022

Idaho National Laboratory
Idaho Falls, Idaho 83415

http://www.inl.gov

Prepared for the
U.S. Department of Energy
Under DOE Idaho Operations Office
Contract DE-AC07-05ID14517

Page intentionally left blank

CONTENTS

ACRONYMS v
1. INTRODUCTION 1
2. METHODS 2
3. RESULTS AND DISCUSSION 8
4. CONCLUSIONS AND FUTURE WORK 13
5. REFERENCES 14

FIGURES

Figure 1. Montage of two images of the same experiment X-419A-T001-149-161-002-126-185 obtained with dysprosium (left) and indium (right) foils. 3
Figure 2. Pixel intensity histograms of the two images of X-419A-T001-149-161-002-126-185 experiment obtained with dysprosium (top) and indium (bottom) foils. 4
Figure 3. Intensity-adjusted image of X-419A-T001-149-161-002-126-185-08 using indium foil. 5
Figure 4. Histogram of the intensity-adjusted image of X-419A-T001-149-161-002-126-185-08 using indium foil. 6
Figure 5. Zoomed-in part of pin #3 (from the left) shown as yellow rectangle on image in Figure 3. 7
Figure 6. Color mapping of the intensity adjusted image of experiment X-419A-T001-149-161-002-126-185-08. 8
Figure 7. Zoomed-in part of the image in Figure 6 shown with red rectangle. 9
Figure 8. Zoomed-in part of pin #3 of experiment X-419A-T001-149-161-002-126-185-08 with U-19Pu-10Zr composition. 9
Figure 9. Color mapping of intensity adjusted image of experiment X-419A-T289-183-173-171-165-075. The pins' fuel composition is shown on top of the image. 10
Figure 10. Pin T289 from experiment X-419A-T289-183-173-171-165-075-36. 11
Figure 11. Zoomed in section of the image of pin T289 shown in Figure 10. 12

Page intentionally left blank

ACRONYMS

BU	burnup
CR	computed radiography
DOE	U.S. Department of Energy
EBR-II	Experimental Breeder Reactor II
FY	fiscal year
INL	Idaho National Laboratory
ITU	International Telecommunication Union
RAM	random access memory
RGB	red, green, blue
SEM	scanning electron microscopy

Page intentionally left blank

Data Mining – Image Analysis of Radiography for Zr Redistribution

1. INTRODUCTION

The research effort described in this report represents a first attempt to investigate the radial redistribution of Zr in ternary fuel alloys U-xPu-10Zr (x = 0, 8, 19) irradiated in the in-reactor fuel experiments during the operation of the U.S. Department of Energy's (DOE's) Experimental Breeder Reactor II (EBR-II) at Idaho National Laboratory (INL) using methods of image processing on post-irradiation neutron radiographs. Approximately 130,000 metal fuel pins were irradiated in EBR-II during its 30 years of operation to develop and characterize existing and prospective fuels. For many of the metal fuel irradiation experiments, neutron radiography imaging was performed historically now allowing application of modern image analysis techniques to characterize fuel behavior, such as fuel swelling, fluff formation, and now, fuel alloy constituent redistribution. The redistribution of fuel components depends on the temperature field, radially, within the fuel [1]. Specifically, Zr is expected to redistribute radially towards the center of the pin, as well as towards the outer zones [1]. Currently, direct imaging of a pin cross-section through optical methods or scanning electron microscopy (SEM) is used to study the constituents' redistribution, which is very time-consuming and can only be applied to a limited number of pins. An automated image processing technique allowing for the investigation of fuel radial redistribution zones would significantly accelerate data analysis. In general, if the fuel temperature is hot enough, three redistribution zones are expected, corresponding to the main fuel components (e.g., U, Pu, Zr) [1]. While more assessment will be performed in fiscal year (FY)-2023, it seems possible to differentiate the pins according to their fuel composition using image analysis techniques on neutron radiographs of metallic fuel pins based on the analysis to date.

2. METHODS

The irradiated metallic fuel pins discussed in this report were radiographed using computed radiography (CR) with indirect conversion indium or dysprosium foil detectors most sensitive to epithermal, or thermal neutrons, respectively. The activated foils were then used to transfer images to film. Dysprosium foil is more sensitive to thermal neutrons and provides images with better contrast at the expense of more shallow penetration of the fuel. The indium foil is more sensitive to epithermal neutrons and provides images with less contrast, but with flatter histograms, as shown below.

A detailed description of neutron radiography imaging can be found in Reference [2]. Images on film were subsequently digitized using a scanner to obtain images in a JPEG format. These JPEG images were used as original images for the image processing algorithms presented in the report. The CR is used to gain insights into the behavior of different fuel components after different degrees of irradiation and burnup (BU). The purpose of this report is to evaluate the possibility of detection of the radial redistribution of Zr, which forms radial zones in the fuel with different compositions. The two EBR-II metallic fuel pins analyzed in this report are X-419A-T001-149-161-002-126-185-08 and X-419A-T289-183-173-171-165-075-36.

The original JPEG images of neutron radiography were acquired with 150 dpi resolution using a 35 mm focal-length camera, which on average have the size of 4,300 by 10,000 pixels with a color depth of 24 bits. The JPEG image format uses a compression algorithm to store the image; however, it is decompressed while being loaded into random access memory (RAM) and takes the same amount of RAM as lossless formats, such as TIFF. The original JPEG images use red, green, blue (RGB) color coding, which requires three bytes to represent each pixel. Since the neutron radiographs have no meaningful color information, the RGB images prior to processing have been converted into grayscale images. Since each channel in an RGB image has 256 shades, the RGB image is converted into grayscale by taking the weighted sum of the R, G, and B values. Specifically, for this paper, the conversion formula, as shown in Equation (1), is:

$$\text{Gray} = 0.2989 \times \text{R} + 0.5870 \times \text{G} + 0.1140 \times \text{B} \quad (1)$$

This triplet of weights (e.g., 0.2989, 0.5870, 0.1140) used in the conversion formula, comes from BT.601-7 [3] recommendations developed by the International Telecommunication Union (ITU). Since all three channels in the grayscale image are set to the same level, only one byte is necessary to store each pixel—thus reducing the RAM requirements by a factor of three. Since the grayscale image pixel values range from 0-black to 255-white, each value in that range is mapped into a shade of gray, with an assumption that black and white colors are extreme representations of gray. The image contrast or intensity is defined as the difference between the brightest and darkest pixels [4].

Figure 1 shows a montage of the two images taken from the same experiment using either dysprosium foil or indium foil. As can be seen from the figure, the dysprosium foil, which is most sensitive to thermal neutrons, produced an image of high contrast with fuel pins having much higher pixel intensity than the background. On the other hand, images produced with epithermal neutrons-sensitive indium foil produced images with significantly less contrast, but with more shades of gray. For this report, the lower contrast images are more useful and were favored over thermal neutron imaging. The reason for this preference is revealed by image histograms, as shown in Figure 2. The top panel shows the histogram of a dysprosium image, which effectively is bimodal with two peaks representing black background and nearly white pins with pixel values over 200. Most importantly, the gray pixel values representing intermediate values of gray color are practically nonexistent in the dysprosium-based image, making it practically a binary image.

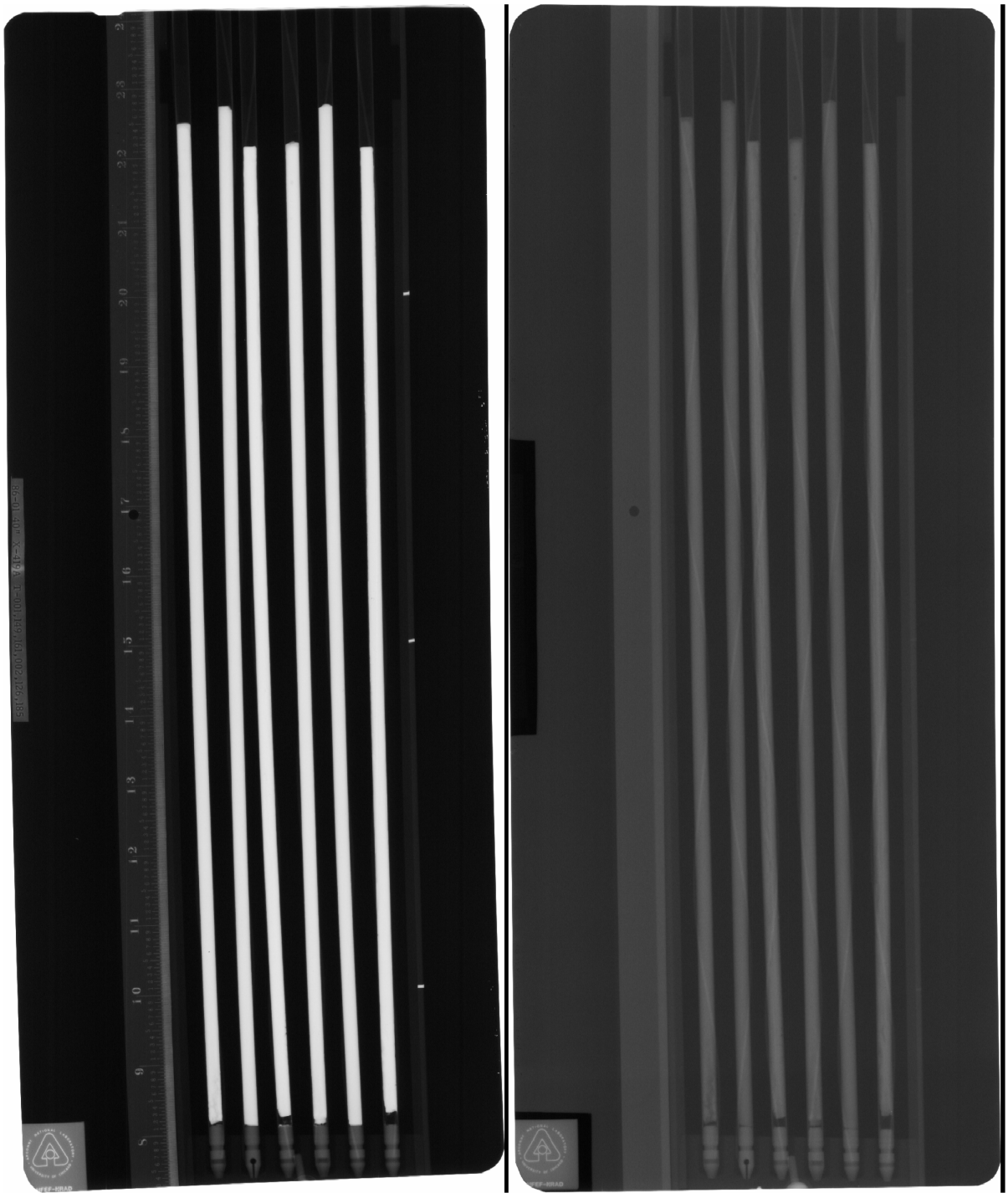

Figure 1. Montage of two images of the same experiment X-419A-T001-149-161-002-126-185 obtained with dysprosium (left) and indium (right) foils.

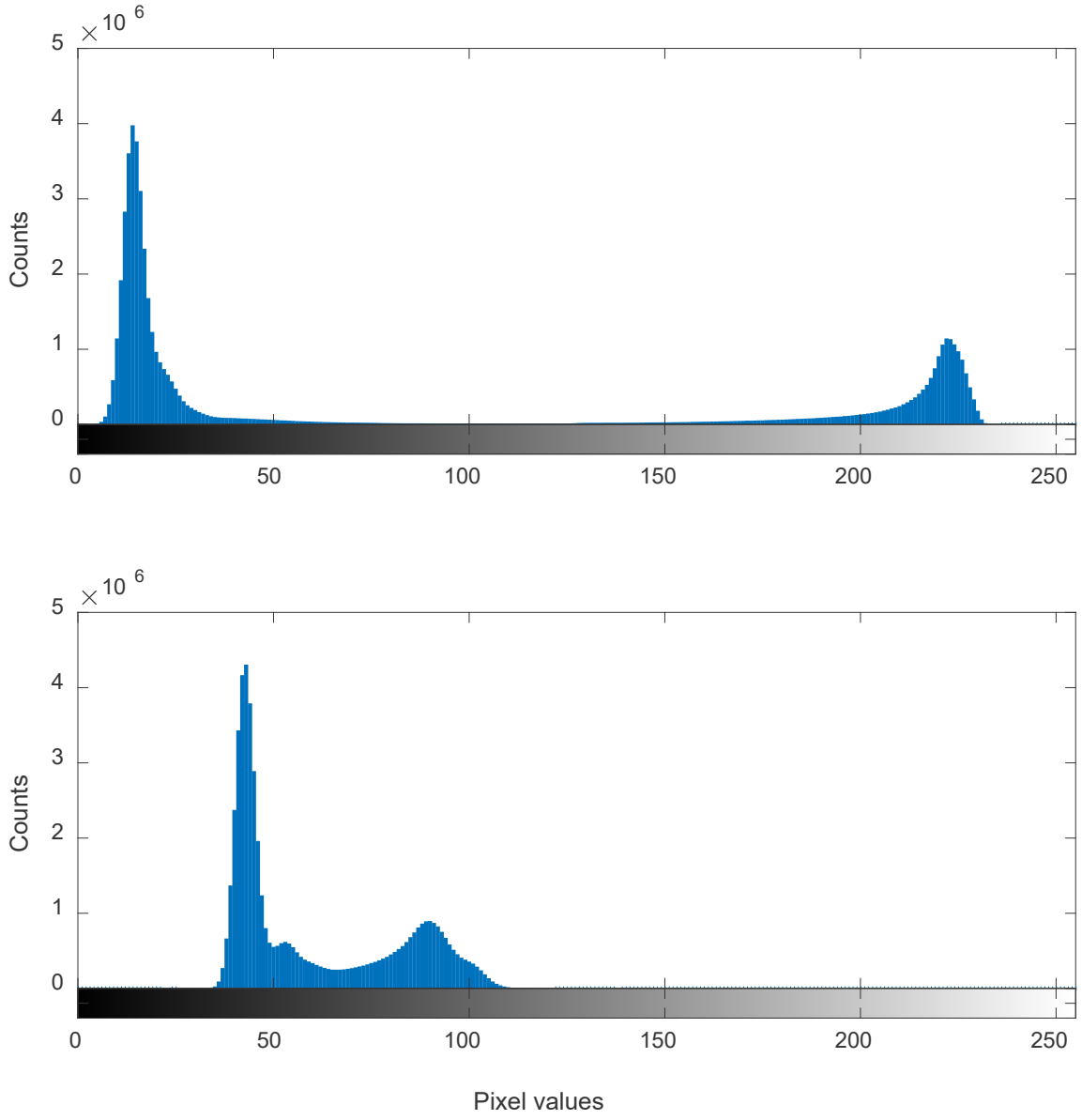

Figure 2. Pixel intensity histograms of the two images in the X-419A-T001-149-161-002-126-185 experiment obtained with dysprosium (top) and indium (bottom) foils.

Such high-contrast images, while useful for segmentation and pattern extraction such as in fuel expansion studies, for example, are of little value when it comes to studying subtle variations in material density. In this case, images with less contrast and more variation in pixel intensity, as shown in the bottom panel of Figure 2, are more useful. While the contrast of the image is lower, it has three modes that may reveal the internal structure of the investigated pin. To improve the quality of the indium foil images, a contrast adjustment procedure has been applied to the image shown on the right panel of Figure 1. To increase image contrast, the enhancement algorithms saturate a given percentage of pixels from the bottom and top of the grayscale—thus stretching the image pixel values. For this report, the saturation limits were set at 15% for the low intensity pixels and 35% for the high intensity pixels, which means that pixels with intensity values less than 38 were mapped to zero, while pixels with intensity values higher than 89 were mapped to 255. The intensity values between 38 and 89 are linearly mapped into the 0 – 255 range. The intensity-adjusted image is shown in Figure 3.

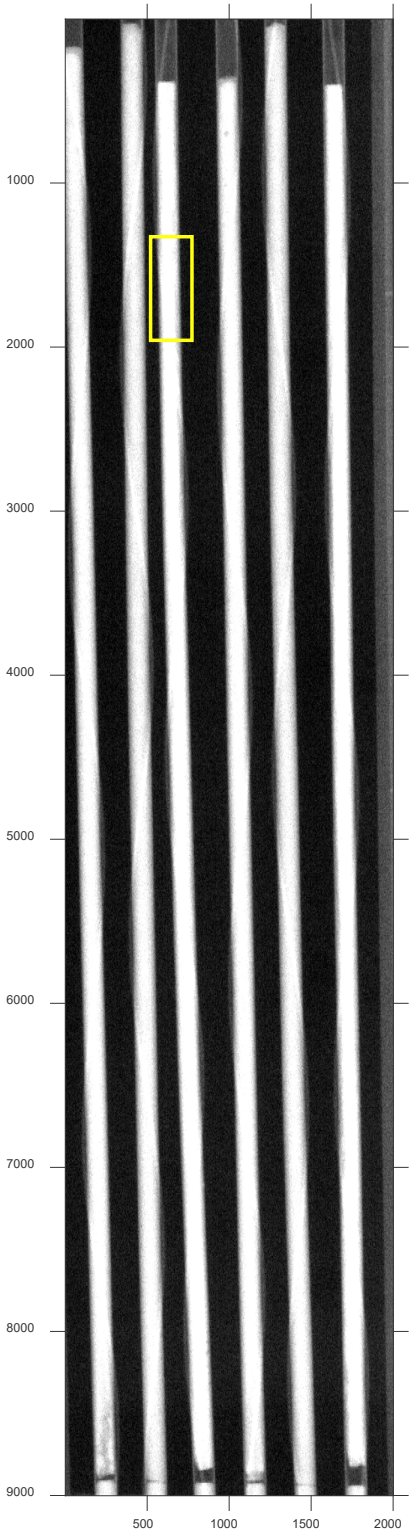

Figure 3. Intensity-adjusted image of X-419A-T001-149-161-002-126-185-08 using indium foil.

As seen from the bottom histogram in Figure 2, the range of pixels between 38 and 89 effectively covers the whole histogram producing a stretched histogram, as shown in Figure 4.

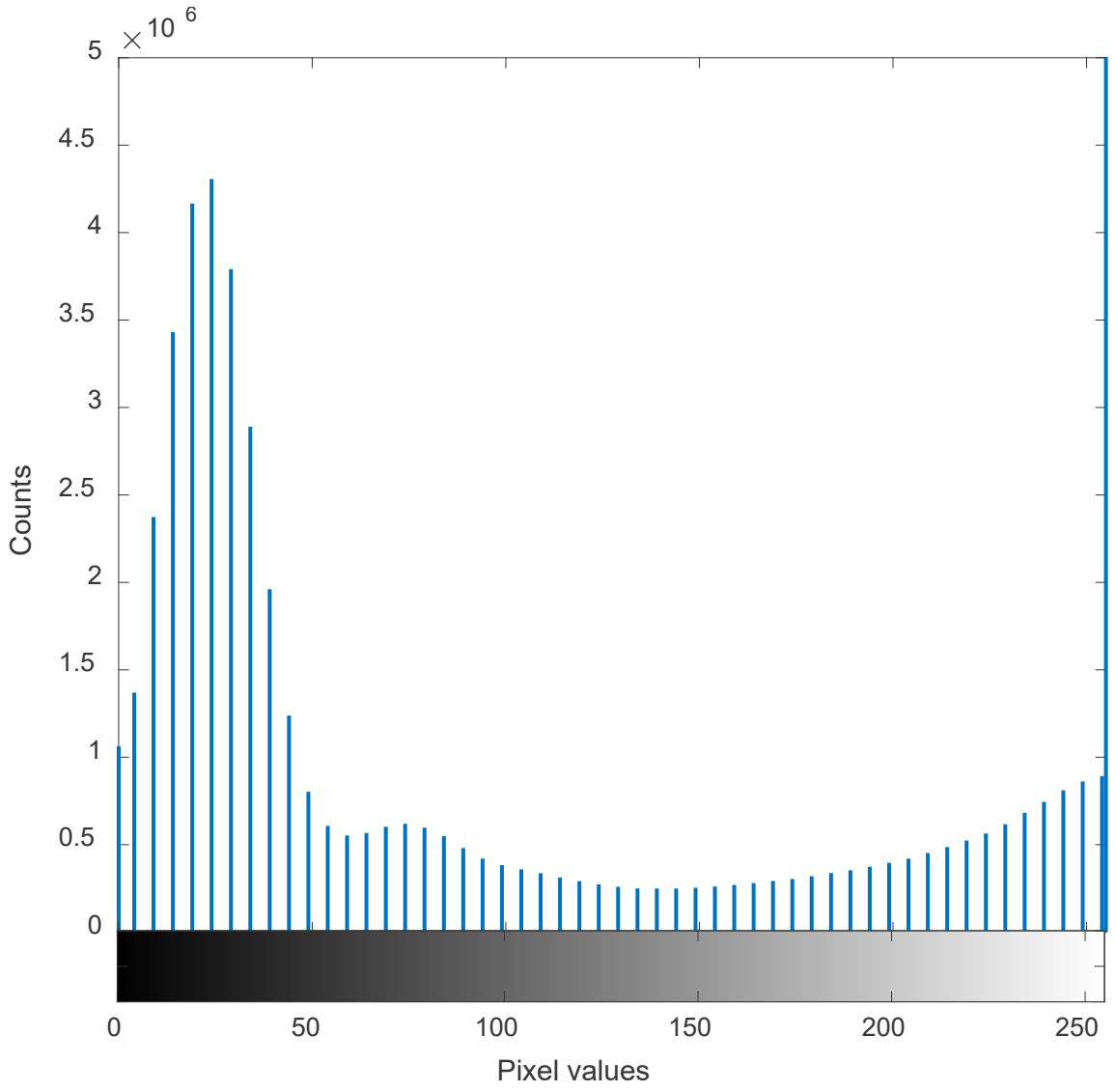

Figure 4. Histogram of the intensity-adjusted image of X-419A-T001-149-161-002-126-185-08 using indium foil.

The benefits of the intensity-adjustment for indium-foil images are obvious in Figure 5.

Figure 5 is a zoomed-in portion of pin #3 from Figure 3 shown as a yellow rectangle. As can be seen from Figure 5, the intensity adjustment reveals lower material density to the right side of the pin, which may be due to material redistribution or BU. The lower-density part is circled with an oval. Figure 5 also intends to demonstrate that the brighter pixels in the center of the pin are not necessarily due to the thickness of the pin in the center, but also due to the material's property. If the pin's thickness was the only parameter affecting the intensity of the pixels, the intensity would be symmetric with respect to the central axis of the pin similar to the bottom part of Figure 5.

The next step in image processing and enhancement used in this report is image color mapping using scaled colors. In the color mapping approach, the image matrix is treated as a color matrix where each element of the matrix specifies the color of the pixel corresponding to a colormap [4]. This representation facilitates visual analysis of the image as the human eye is most sensitive to yellow-green colors, not to the shades of gray [5].

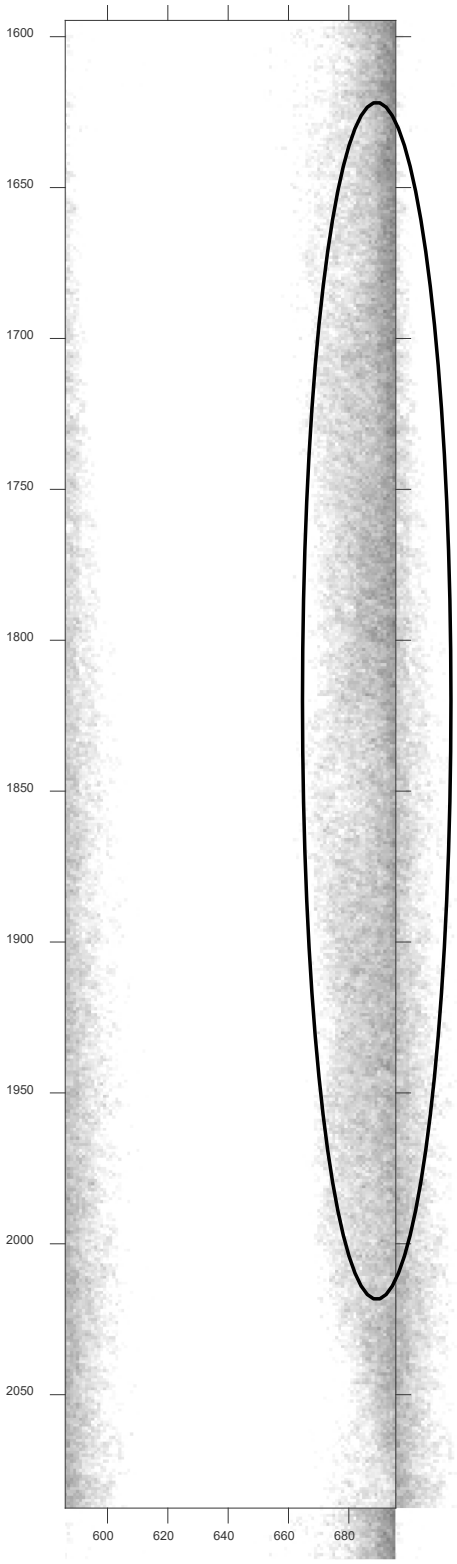

Figure 5. Zoomed-in part of pin #3 (from the left), which was shown as the yellow rectangle on the image in Figure 3.

3. RESULTS AND DISCUSSION

The color mapped image of experiment X-419A-T001-149-161-002-126-185-08 using indium foil is shown in Figure 6. The fuel compositions of the pins for the experiment are U-8Pu-10Zr, U-10Zr, U-19Pu-10Zr, U-8Pu-10Zr, U-10Zr, and U-19Pu-10Zr moving from left to right (i.e., the leftmost pin's fuel composition is U-8Pu-10Zr, the second leftmost is U-10Zr and so on). The experiment X-419A-T001-149-161-002-126-185-08 has pins with all three most common fuel compositions, and thus, is very appropriate for the analysis. The average BU percentage for this experiment was 2.4%. The color mapping bar next to the image in Figure 6 demonstrates that pixels with lower values are mapped in blue colors while pixels with higher values are mapped into yellow colors. An analysis of Figure 6 shows that pins #3 and #6 with the highest plutonium content have a more intense, longitudinal yellowish core in the middle of the pins.

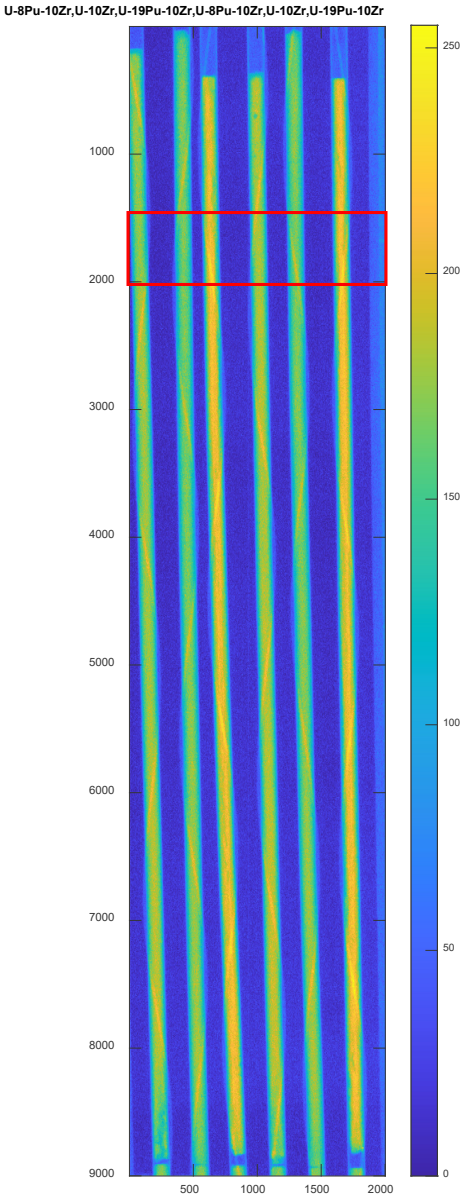

Figure 6. Color mapping of the intensity-adjusted image of experiment X-419A-T001-149-161-002-126-185-08.

Meanwhile, for pins #1 and #4 with 8 wt.% Pu, the yellow core is less intense. The yellow core is practically absent in pins #2 and #5, which have no Pu content. This observation is confirmed by Figure 7, which shows the zoomed-in portion of Figure 6 marked with the red rectangle.

As can be seen in Figure 7, the two pins with the highest Pu concentration stand out with vibrant yellow cores, while the yellow color in the middle of the other pins is less intense with U-10Zr having a practically greenish-yellow core. Figure 8 shows pin #3 from Figure 7 separately to better reveal its color mapping. As can be seen from Figure 8, the color mapping clearly shows three different radial regions corresponding to the yellowish innermost region, greenish intermediate region, and light blue outermost region. Notice that if the more intense, higher pixel values were exclusively associated pin thickness being larger in the middle, all pins would have a similar yellow inner region regardless of the fuel composition.

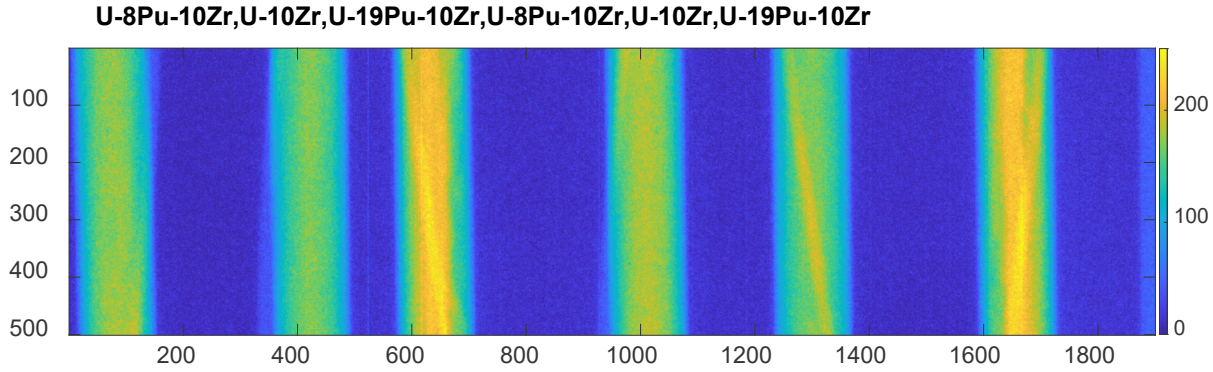

Figure 7. Zoomed-in part of the image in Figure 6 shown with a red rectangle.

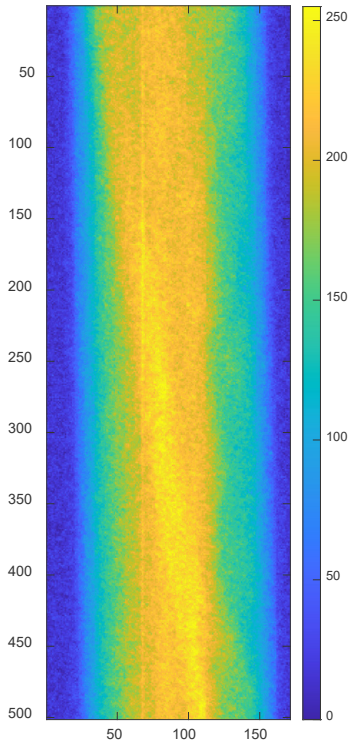

Figure 8. Zoomed-in part of pin #3 of experiment X-419A-T001-149-161-002-126-185-08 with U-19Pu-10Zr composition.

Another example of color mapping for a different experiment of X-419A-T289-183-173-171-165-075-36 is shown in Figure 9. The raw image was obtained with indium foil and was processed with the same technique of contrast enhancement as the previous image. The fuel compositions for the pins in this image moving from left to right were U-19Pu-10Zr, U-19Pu-10Zr, U-19Pu-10Zr, U-19Pu-10Zr, U-19Pu-10Zr, and U-10Zr. The first pin from the left, T289, was selected for a more detailed analysis as it has shown a prominent structure on the color-mapped image. The T289 pin was at 0.7 BU%. Figure 10 shows pin T289 as a color-mapped image. The pin has three color regions: (1) inner with greenish color; (2) intermediate with yellowish color; and (3) the outer region again of greenish color. For an easier visual analysis, part of the image in Figure 10 between the y coordinates of 1000 and 4000 is zoomed in and shown in Figure 11, which shows both an intensity-enhanced gray-scale image in the right panel and a color-mapped image in the left panel. In the left panel, a prominently darker core is clearly visible; however, it is difficult to discern any other regions based on this image. On the other hand, the color-mapped image on the left shows a greenish core, yellowish intermediate region, and greenish outer region. According to the three-regions hypothesis, the central and outer regions should have higher Zr concentrations, while the intermediate region should have a higher U concentration. In this case, the color mapped image in Figure 11 may be displaying those regions.

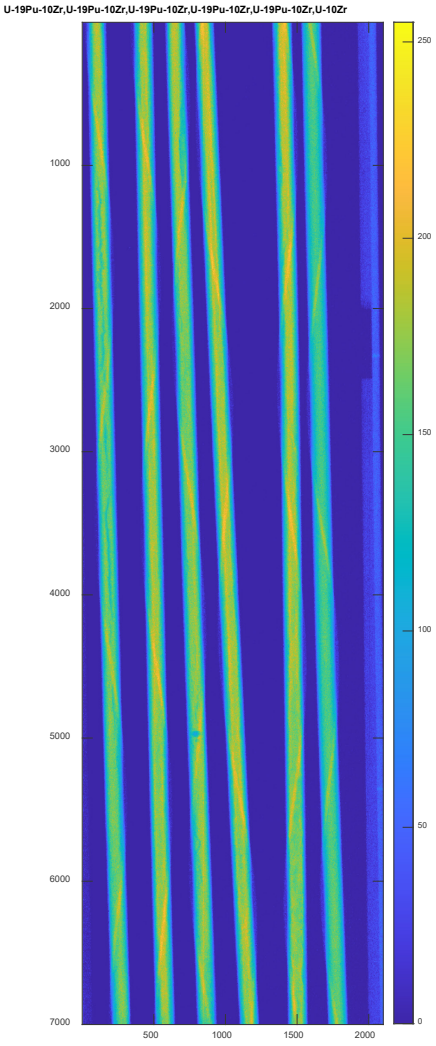

Figure 9. Color mapping of the intensity-adjusted image of experiment X-419A-T289-183-173-171-165-075. The fuel composition of the pins is shown on top of the image.

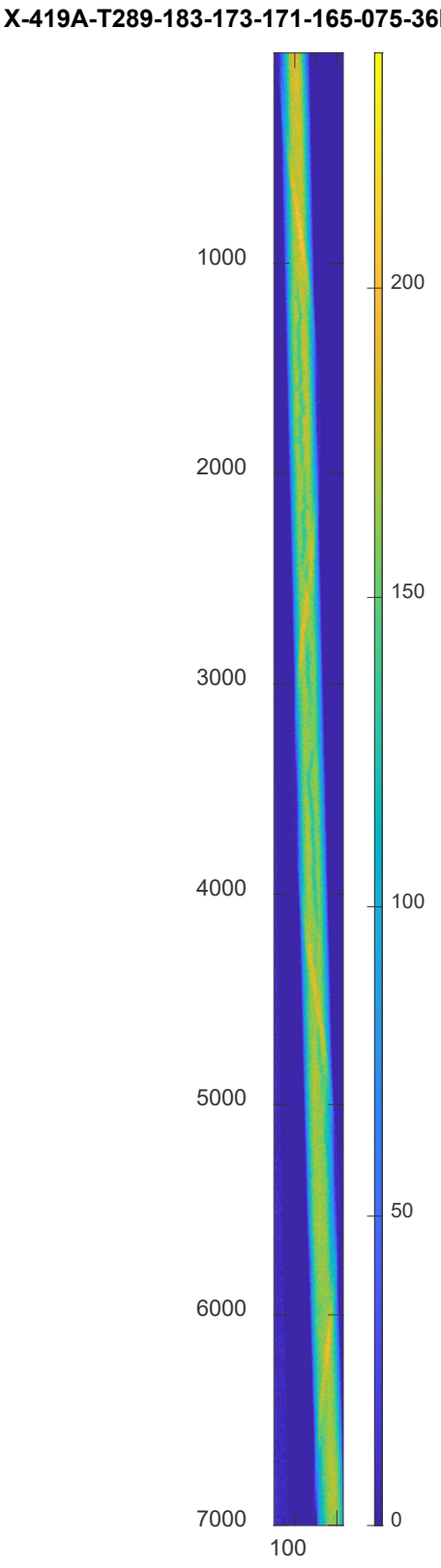

Figure 10. Pin T289 from experiment X-419A-T289-183-173-171-165-075-36.

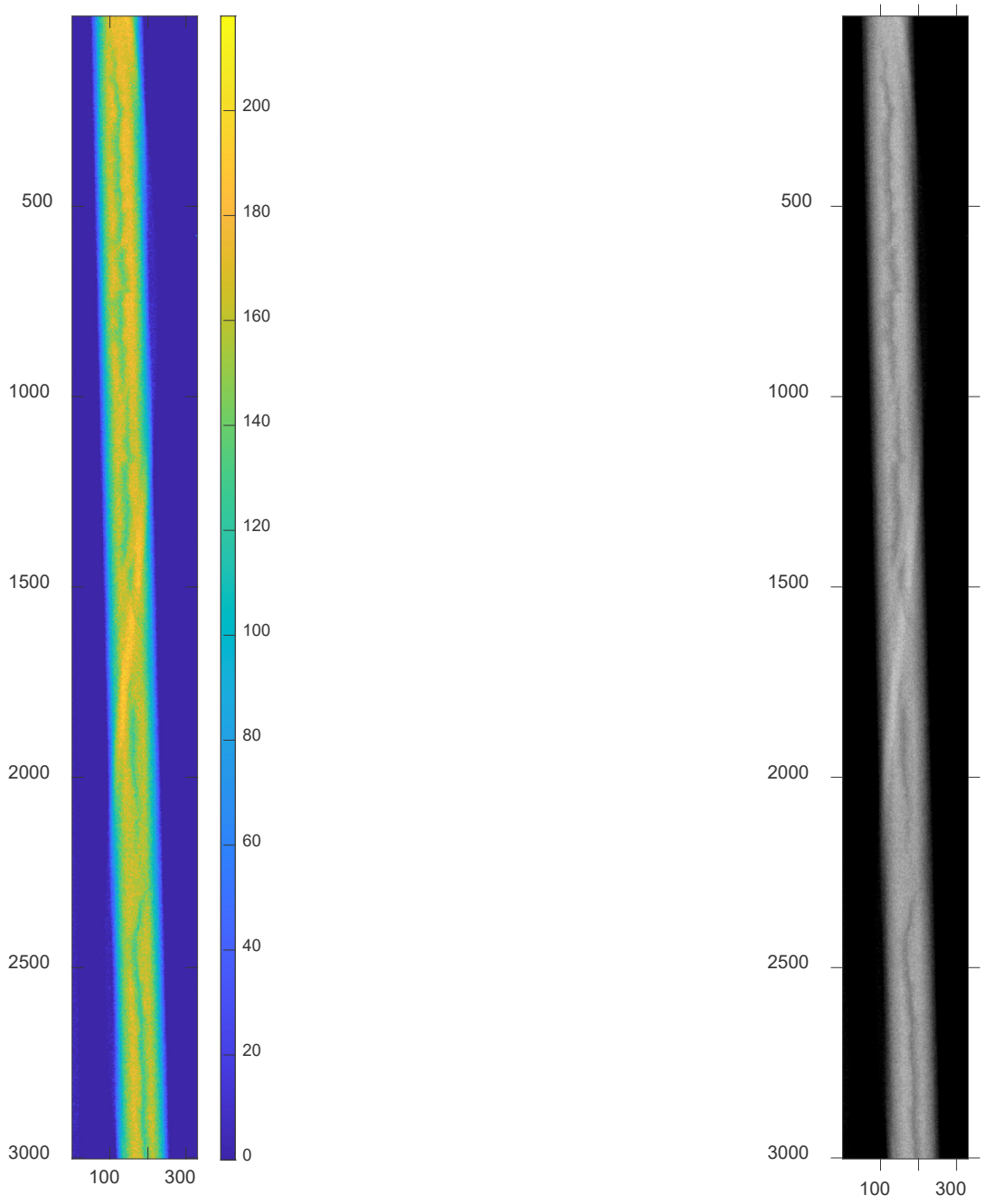

Figure 11. Zoomed in section of the image of pin T289 shown in Figure 10.

4. CONCLUSIONS AND FUTURE WORK

This report presents the initial results of the analysis on the neutron radiography images obtained with indium foil to investigate the redistribution of fuel alloy constituents. The purpose of the analysis was to explore the possibilities of studying the Zr redistribution in fuel pins using image processing and computer vision techniques. The current approach to studying fuel behavior in irradiated pins is to section pins at various lengths and analyze the cross-sections through either optical microscopy or SEM. This examination is destructive and time-consuming and typically limited to a few cross-sections along the axial fuel length. The applicability of a nondestructive examination for studying Zr redistribution will allow for a quick analysis of many pins, thus significantly increasing the amount of data available for fuels modeling and development.

The results presented in this report show an analysis of two radiography images with 12 total pins. The pins have different fuel compositions and different BU percentages. It is shown that by applying standard image processing techniques, such as image enhancement and image color mapping, it is possible to localize and visualize at least three different regions within a pin's radial profile. The typical three-zone characteristic of irradiated metallic fuels corresponds with predominant concentrations of specific fuel constituents.

Whether these regions can be associated with redistribution of fuel components requires further investigation and will be performed by comparison of color mapped images with different BU percentages. However, based on the analysis to date, it seems possible to differentiate the pins according to their fuel composition based on the number of pixels in the yellow region (e.g., pixel values higher than 200). A negative result, in terms of whether this reveals the zone formation, is that there does not seem to be an axial change in the radial position of image density, as would be expected due to operating temperature differences axially along the pin.

Future work will include the following tasks with the goal of first proving the methodology:

1. The application of more sophisticated image processing techniques, such as filtering, deblurring, segmentation, and edge detection to radiography images. These techniques can significantly improve signal-to-noise ratio and allow the detection of features, which are not readily available in the raw images. Methods of normalizing the two-dimensional (2D) radiography of a three-dimensional (3D) object may also be explored (i.e., thickness effects, zone layering).
2. The comparison of the results of fuel behavior obtained through image processing of radiographs with the results obtained through optical microscopy or SEM of the pin cross-sections. Several pins have been radiographed first and later subjected to destructive examination. Those pins can be used for comparison as destructive microscopy examination can serve to validate the image processing analysis results.
3. Image analysis of the same pin through different BU percentages to reveal the changes in fuel redistribution due to increasing BU percentages.
4. With a proven method, several applications are envisioned to existing and future radiography images that will greatly enhance metallic fuel performance understanding.

5. REFERENCES

1. Porter, D. L., and H. Tsai, 2011, "Full-length Metallic Fast Reactor Fuel Pin Test in FFTF (IFR-1)," INL/LTD-11-21062, Idaho National Laboratory, Idaho Falls, ID, USA.
2. Craft, A. E., G. C. Papaioannou, D. L. Chichester, and W. J. Williams, 2017, "Conversion from film to image plates for transfer method neutron radiography of nuclear fuel," *Physics Procedia* 88, 81–88. https://doi.org/10.1016/j.phpro.2017.06.010.
3. International Telecommunication Union (ITU), 2011, "BT.601: Studio encoding parameters of digital television for standard 4:3 and wide screen 16:9 aspect ratios," ITU, Geneva, Switzerland. https://www.itu.int/rec/R-REC-BT.601/.
4. Gonzalez, R. C., and R. E. Woods, 1992, *Digital Image Processing*, 3rd Edition, Addison-Wesley, Boston, MA, USA.
5. Robinson, S. J., and J. T. Schmidt, 1984, "Fluorescent penetrant sensitivity and removability – What the eye can see, a fluorometer can measure," *Materials Evaluation* 42(8), 1029-1034. https://doi.org/10.1016/j.phpro.2017.06.010.